Resonant inelastic x-ray scattering at the N₂ π* resonance: Lifetime-vibrational interference, radiative electron rearrangement, and wave-function imaging

L. Kjellsson [1,2,*] V. Ekholm,[3] M. Agåker [1,3] C. Såthe,[3] A. Pietzsch,[4] H. O. Karlsson [5] N. Jaouen,[6] A. Nicolaou,[6] M. Guarise,[7] C. Hague,[8] J. Lüning,[8,9] S. G. Chiuzbăian [8] and J.-E. Rubensson [1,†]

[1]*Department of Physics and Astronomy, Uppsala University, Box 516, SE-751 20 Uppsala, Sweden*
[2]*European XFEL GmbH, Holzkoppel 4, 22869 Schenefeld, Germany*
[3]*MAX IV Laboratory, Lund University, Box 118, Lund SE-221 00, Sweden*
[4]*Helmholtz Zentrum Berlin, Institute Methods and Instrumentation for Synchrotron Radiation Research,
Albert-Einstein-Straße 15, 12489 Berlin, Germany*
[5]*Department of Information Technology, Uppsala University, Box 337, SE-751 05 Uppsala, Sweden*
[6]*Synchrotron SOLEIL, Saint-Aubin, Boite Postale 48, 91192 Gif-sur-Yvette Cedex, France*
[7]*Brazilian Center for Research in Energy and Materials (CNPEM), Rua Giuseppe Máximo Scolfaro,
10.000 Polo II de Alta Tecnologia de Campinas, Campinas, São Paulo, Brazil*
[8]*Sorbonne Université, CNRS, Laboratoire de Chimie Physique-Matière et Rayonnement, F-75005 Paris, France*
[9]*Helmholtz-Zentrum Berlin für Materialien und Energie, Hahn-Meitner-Platz 1, 14109 Berlin, Germany*

Resonant inelastic x-ray scattering spectra excited at the π*-resonance of the nitrogen molecule are presented. Well-resolved vibrational excitations in the electronic ground state, and in the $3\sigma_g^{-1} 1\pi_g^1 \, a^1\Pi_g$ state are observed. The spectra are analyzed within the Kramers-Heisenberg formalism, and the importance of lifetime-vibrational interference effects is highlighted. In addition, strongly dissociative multiply excited final states populated in radiative electron rearrangement are found in the valence ionization continua. The vibrational wave functions of the core-excited state are imaged on the strongly dissociative final state potentials.

I. INTRODUCTION

Nitrogen, N₂, is arguably one of the most studied molecules. It is typically used as a showcase when new techniques are introduced, and it is ubiquitous in development of soft x-ray spectroscopy. Early on it was the first system where vibrational resolution was demonstrated in x-ray emission spectroscopy (XES) [1] and the vibrationally resolved x-ray absorption spectrum (XAS) is often used for determining the resolving power [2–4] and energy calibration of monochromators at synchrotron radiation facilities. Methodological developments still lead to the uncovering of new states and processes in the nitrogen molecule, e.g., in connection with double-core hole excitation dynamics at synchrotrons and [5] and free-electron lasers [6]. Recently it was shown that new core excited states can be investigated in the XAS of the N₂⁺ cation using ion-trap techniques [7]. In resonant photoemission, vibrational resolution was demonstrated in spectra of the nitrogen molecule [8] and new refinements of the technique constantly unveil new states of the ion [9,10].

Early resonant inelastic x-ray scattering (RIXS) measurements by Glans *et al.* [11] addressed lifetime-vibrational interference (LVI) effects, and excitation-emission dynamics close to the ionization thresholds has also been studied in RIXS [12]. In LVI multiple paths to the final state interfere, affecting the scattering process. While LVI has been thoroughly investigated in the electronic decay channel [13], it was not until the latest decade that spectral quality allowed detailed studies in RIXS [14], and vibrationally resolved spectra of free molecules are still scarce.

Here we present vibrationally resolved RIXS spectra excited at the N₂ π* resonance. The resolution allows for a detailed analysis of the vibrational fine structure in the scattering to the electronic ground state and the first dipole-allowed excited state. We discuss significant LVI effects by comparing the results of a full Kramers-Heisenberg (KH) treatment and a two-step absorption-followed-by-emission model. We find an excellent agreement with the predictions of KH theory, and that inclusion of LVI effects is essential to understand the spectra. The implications for the scattering dynamics are briefly discussed.

We also observe the population of multiply excited states in the valence ionization continua. This can be understood in terms of radiative electron rearrangement (RER) in the emission step of the RIXS process [15,16]. RER in the x-ray emission of π* excited N₂ was predicted some time ago [16], and transitions to these multiply excited *gerade*

*ludvig.kjellsson@physics.uu.se
†jan-erik.rubensson@physics.uu.se

TABLE I. The spectroscopic constants used for the Morse potential energy curves are taken from Refs. [19,20,24,25]. The curves and corresponding wave functions are drawn in Fig. 2. E_{00} is the energy from the lowest vibrational level of the ground state to the lowest vibrational level of the excited state, ω_e is the vibrational energy, $\omega_e\chi_e$ is the anharmonicity, R_e is the equilibrium internuclear distance, and Γ is the lifetime broadening.

State	E_{00} (eV)	ω_e (meV)	$\omega_e\chi_e$ (meV)	R_e (Å)	Γ (meV)
Ground state		292.42 [20]	1.78 [20]	1.09768 [20]	
$1\sigma_u^{-1}1\pi_g^1$	400.88 [19]	236.08 [19]	2.14 [19]	1.1641 [24]	115 [25]
$3\sigma_g^{-1}1\pi_g^1$	8.55 [20]	210.05 [20]	1.72 [20]	1.2203 [20]	

states are now observed. We find that these states are strongly dissociative and we demonstrate that that the RIXS spectra effectively map the vibrational wave functions in the intermediate core excited state.

II. METHOD

RIXS spectra of gas-phase nitrogen were measured using the AERHA spectrometer [17] at the SEXTANTS beamline [18] at the SOLEIL synchrotron. A 1000 Å thick diamondlike carbon membrane with width and length 0.5 and 3 mm, respectively, was used to separate the close-to-atmospheric sample pressure in a gas-cell from the ultrahigh vacuum. This arrangement has been used in several similar studies. The angle between the incident radiation and the membrane surface was $45°$, and the scattering angle was $85°$.

The absolute energy of the beamline monochromator was calibrated by a fluorescence yield measurement of the N_2 resonance, using a microchannel plate detector mounted mounted $45°$ above the scattering plane, in the plane of the incident radiation. The first vibrational absorption peak was aligned to the literature value, 400.88 eV [19]. The spectrometer energy dispersion was calibrated to be linear in wavelength by fixing the energy difference of the $v = 0$ peaks of the ground state and the first electronically excited state to 8.55 eV [20].

The incident energy was scanned over the nitrogen π^* resonance [19] from higher to lower energies in the 402.5–400.5 eV range in 39 steps, while accumulating RIXS spectra for 5 minutes at each energy. The sample was frequently moved in the vertical direction to avoid membrane rupture due to radiation damage. The monochromator exit slit was set to 20 μm, resulting in an elastic peak with around 150 meV FWHM.

To model the vibrational spectra we first use the Born-Oppenheimer approximation to separate the electronic and vibrational wave functions. Second-order perturbation theory leads to the Kramers-Heisenberg formula, which is often used to describe the RIXS process [21]. All vibrational states $|n\rangle$ in the intermediate core-excited state contribute to the scattering. The intensity of the scattered radiation as a function of excitation energy E_{exc}, for each vibrational final state $|f\rangle$, is given by [22]

$$I_f(E_{exc}) \propto M(E_{exc})\left|\sum_n \frac{\langle f|n\rangle\langle n|g\rangle}{E_{exc} - (E_n - E_g) + \frac{i\Gamma}{2}}\right|^2, \quad (1)$$

where $|g\rangle$ is the initial state, Γ is the lifetime width of the intermediate state, E_n and E_g are the energies of the inter-

mediate and ground states, respectively, and $M(E_{exc})$ is the monochromator function, describing the energy distribution of the incident radiation. To highlight the interference effects we investigate a "two-step" expression for reference. This expression contains the sum of the squares, rather than the square of the sum, and thereby the interference effects are turned off:

$$I_{f,2step}(E_{exc}) \propto M(E_{exc})\sum_n \left|\frac{\langle f|n\rangle\langle n|g\rangle}{E_{exc} - (E_n - E_g) + \frac{i\Gamma}{2}}\right|^2. \quad (2)$$

Thus, the interference contribution is simply $I_f - I_{f,2step}$. Morse potential curves were calculated using the parameters in Table I, and the corresponding wave functions were calculated using the analytical procedure from [23].

RIXS spectra were calculated using (1) and (2) over incident energies in the 400–404 eV range. We assume that $M(E_{exc})$ is Gaussian with 70 meV FWHM. As this width is similar to the width of the resonances, (1) and (2) predict that the peaks are slightly shifted from their nominal energies. For the comparison we have shifted the elastic peak of both experiment and theory to the nominal zero-energy loss. Finally, the theoretical spectra were convoluted by a Gaussian with 150 meV FWHM, corresponding to the resolution of the spectrometer.

III. RESULTS AND DISCUSSION

A. Lifetime-vibrational interference

We present an overview of the experimental results, along with the predictions in RIXS maps on the energy loss scale in Fig. 1. On the left, the projection of the RIXS map on the incident energy scale is shown (red line) together with the partial fluorescence yield (PFY) spectrum (black line). The distortion in the projected spectrum, especially obvious in the attenuation of the signal just above 401 eV incident energy, is an artifact probably due to the varying position of the membrane relative to the photon beam during the RIXS map measurements. Dashed lines mark the vibrational maxima in the π^* resonance to guide the eye.

We observe transitions to two electronic final states with vibrational fine structure. We assign the elastic peak at zero energy loss to scattering to the electronic-vibronic ground state, $1\sigma_g^2 1\sigma_u^2 2\sigma_g^2 2\sigma_u^2 1\pi_u^4 3\sigma_g^2\ ^1\Sigma_g^+$, and the progressions of energy-loss peaks up to 3 eV to vibrational excitations. At 8.55 eV energy loss we observe scattering to the vibrational ground state of the dipole-allowed $3\sigma_g^{-1}1\pi_g^1\ a^1\Pi_g$ state, together with a progression of vibrational excitations at higher-energy losses. This state is associated with the
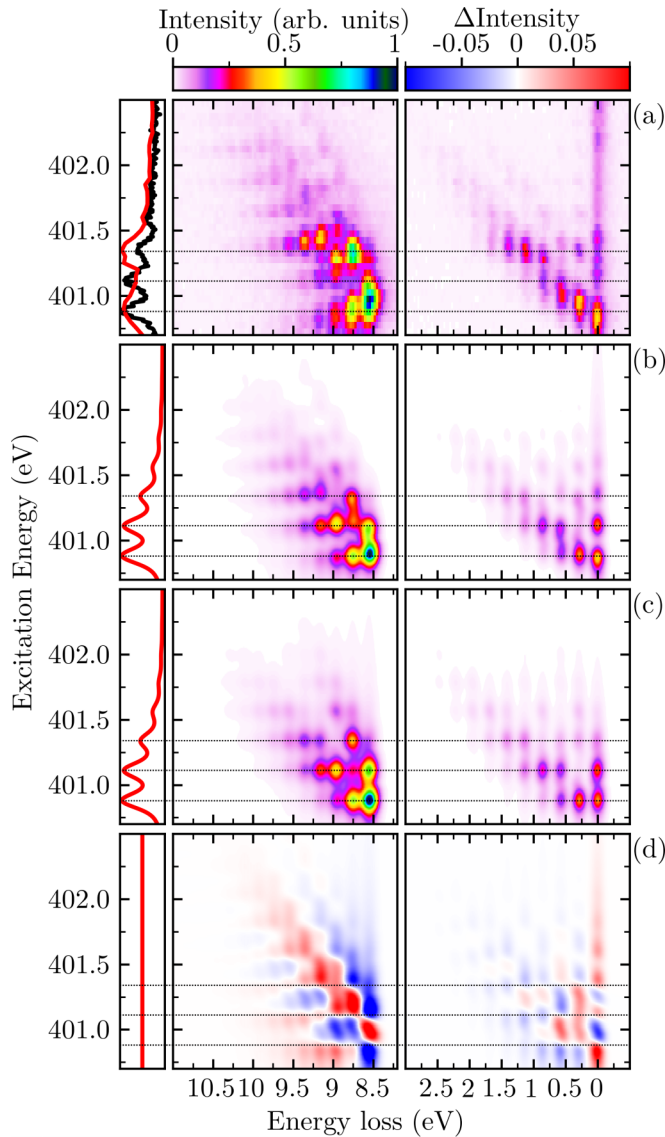
FIG. 1. RIXS maps covering the N_2 π^* resonance. Projection of the spectra on the left represents partial fluorescence yield. Experimental data (a) are shown together with predictions including interference effects (b), disregarding interference (c), and the interference terms shown separately (d). As LVI redistributes intensity they comprise both positive (red) and negative (blue) regions. Dashed lines are drawn on the π^* vibrational resonances for clarity.
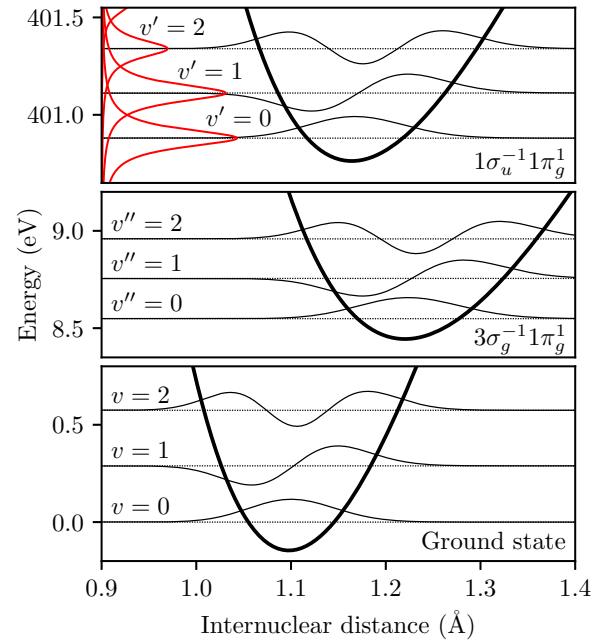

FIG. 2. Morse potential energy curves based on the values in Table I are shown together with the first vibrational energy levels and corresponding wave functions. The intrinsic lifetime widths of the intermediate states are indicated by red Lorentzians.

Lyman-Birge-Hopfield band system in the vacuum ultraviolet (VUV) region [26]. For both electronic final states we see increasing vibrational final-state excitations as the incident photon energy increases, in accordance with the predictions (Fig. 1). Although significant differences between the predictions with and without LVI are found, the effects are not very pronounced.

In N_2 the separation between the vibrational levels in the core excited state is larger than the core-hole lifetime broadening (Table I). Therefore the LVI effects are manifested in a somewhat different way from the corresponding π^* resonance in O_2, where the lifetime broadening is larger than the separation.

In Fig. 2 we compare the Lorentzian width of the core excited states (red lines) with the spacing of the vibrational peaks. While on-resonance excitation is dominated by one vibrational wave function, the neighboring vibrational levels have a clear overlap due to the lifetime broadening, and LVI is emphasized for excitations in these regions. This is demonstrated in Fig. 1(d), where it is seen that LVI does not influence the peak positions of the strongest resonances, but introduces an asymmetry as intensity is added or subtracted in between the peaks.

When exciting to the second vibrational resonance $v' = 1$, at 401.35 eV, we notice that the first vibrationally excited state in the electronic ground state $v = 1$ is virtually missing in the experimental data. This is in agreement with predictions, although calculations including LVI show slightly higher intensity in this region compared to calculations that disregard LVI. The "missing" feature can be understood by considering the wave functions (Fig. 2). The displacement of the potential curve of the core excite state is almost one quarter of a wavelength of the nuclear wave function, which leads to a partial cancellation in the Franck-Condon factors for transitions where the vibrational quantum number is the same in the intermediate and final states.

In Fig. 3 we see that the agreement between experimental data and predictions is very good, especially at lower excitation energies.

We attribute the remaining discrepancies to uncertainties in the $M(E_{exc})$ and the broadening due to the limited spectrometer resolution. We note that asymmetries introduced by the LVI and portrayed by the monochromator contribution cause a slight decrease in the observed vibrational spacings.
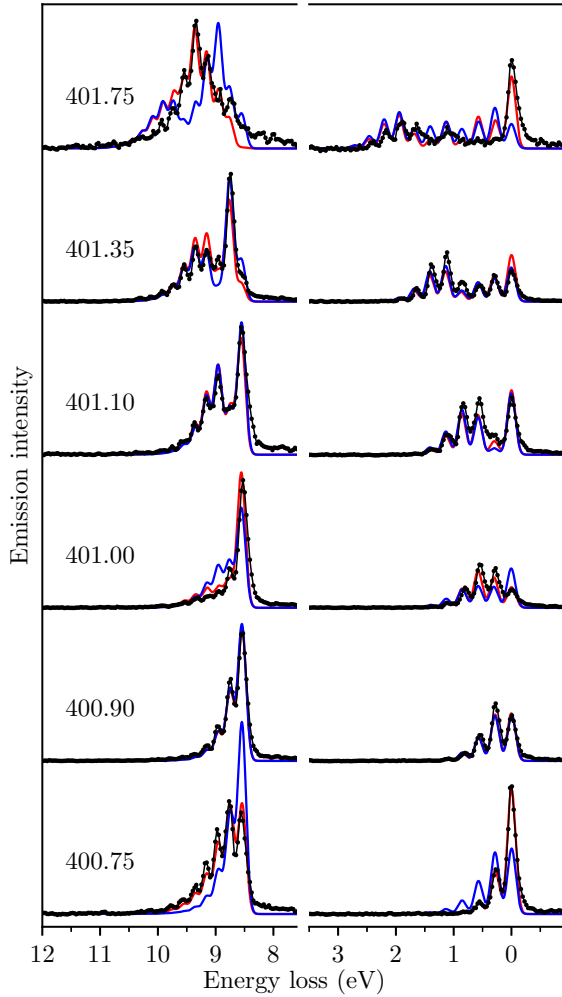
FIG. 3. Selected RIXS spectra (black connected dots) with excitation energies in electron volts as indicated in the figure. The models are shown with interference (red lines), and without interference (blue lines). The interference effects are weakest on the resonances, and strongest for interresonance excitation.

Finally, we note that LVI relates to scattering dynamics, and especially to the evolution of the intermediate-state vibrational wave function in time-dependent scattering theory [21]. For the O_2 π^* resonance this is especially obvious [24], and it has also been demonstrated earlier for N_2 [11]. The present result is in agreement with these studies, and it is particularly obvious at the incident energy of 401.75 eV (Fig. 3) that the prediction which does not include LVI gives main intensity to a different region than the full prediction. As for O_2 these two regions can be associated with the classical inner and outer turning points in the intermediate states. With LVI the limited time for wave-function evolution is reflected in the emphasis of the two different regions.

B. Radiative electron rearrangement and wave-function imaging

Weak broad features, showing a strong excitation-energy dependence, are observed in the 10–25 eV energy-loss range [Fig. 4(a)]. We assign this intensity to multiply excited final
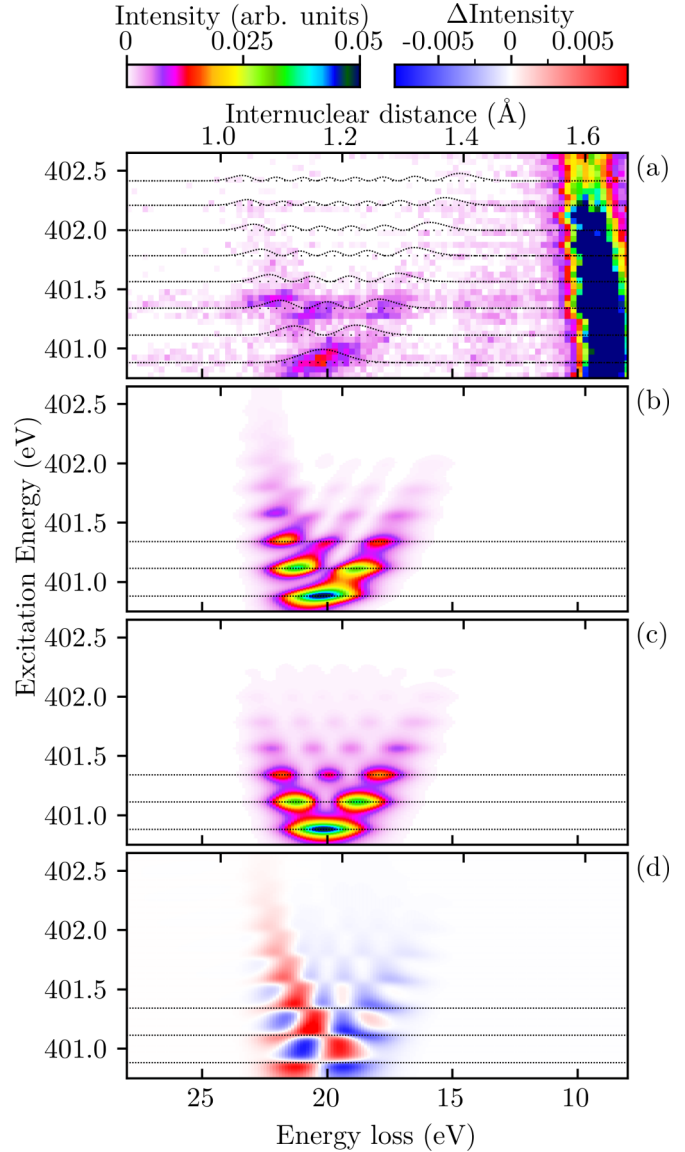

FIG. 4. A RIXS map emphasizing the weak features in the 10–25 eV energy-loss range is shown in (a). We observe a V-shaped feature with its tip around 20 eV energy loss for resonant excitation at $v' = 0$, and weaker intensity at around 14 eV energy loss (energy scale at the bottom of the figure). The squared vibrational wave functions of the intermediate state on the internuclear-distance scale at the top of the figure are included at their resonance energies. Below 10 eV energy loss the already discussed intensity assigned to transitions to the $3\sigma_g^{-1}1\pi_g$ state appears. Theoretical predictions including LVI are shown in (b), and the squared vibrational wave functions of the intermediate states are shown in (c). In (d) the difference between (b) and (c) demonstrate how the LVI effects introduce an asymmetry in line with the observations. The resonance energies are marked as horizontal lines in (b)–(d).

states reached via RER. Although multiple excitations like shake-up/shake-off and radiative Auger in x-ray emission have been investigated [15,27] early on, we are only aware of a few such experimental gas-phase studies [28]. Radiative Auger processes have also been highlighted in coincidence measurements [29]. In RIXS we have earlier also observed

anomalously strong one-photon–two-electron excitations in CO [30] due to interaction between singly and doubly excited states.

For N_2 it is well known that multiply excited final states contribute to the VUV absorption spectrum in this energy range [31,32], and there are several multiply excited ionic states which can be reached in direct photoemission [33–36], and in the electronic decay of the $1\sigma_u^{-1}1\pi_g$ state [9,10]. Indeed, RER transitions to multiply excited states in the decay of the N_2 π^* state were predicted some time ago by Ågren *et al.* [16]. They predict intensity at 380 eV emission energy (23 eV energy loss) to a state with the leading configuration $2\sigma_u^{-1}1\pi_u^{-1}2\pi_g^2$, where the $2\pi_g$ orbital has Rydberg character. The prediction gives this state around 10% of the one-electron transition to the $3\sigma_g^{-1}1\pi_g$ state, which is within the experimental uncertainty. The experimental intensity ratio between the features when exciting at 400.9 eV is 0.05 : 1.0 : 0.52. Thus, the prediction is fully in line with the observations and it would be tempting to assign the intensity in this region accordingly. A final state with the main configuration $1\pi_u^{-1}2\pi_u$ is predicted to get 4% of the $3\sigma_g^{-1}1\pi_g$ intensity at 387 eV emission energy (16 eV energy loss). We observe a very weak feature in the 13–14 eV energy range (Fig. 4), and we speculate that this may be related to the predicted final state.

Note, however, that these assignments imply substantial RER. Although the $1\pi_g$ orbital becomes populated in the intermediate-state excitation, it is not populated in the leading final-state configurations. The configuration for the most intense feature instead implies a three-electron transition in the second step of the scattering process. There are several configurations which may be expected to have larger contributions to the RIXS process. In valence photoelectron spectroscopy it is well known that $3\sigma_g^{-1}$ configuration mixes with the $2\sigma_u^{-1}1\pi_u^{-1}1\pi_g$ configuration [34], and in the present case one would similarly expect a strong mixing between the $3\sigma_g^{-1}1\pi_g$ configuration and $2\sigma_u^{-1}1\pi_u^{-1}1\pi_g^2$. The intuitively simplest symmetry-allowed RER transition would be to $3\sigma_g^{-2}1\pi_g^2$ final states, which could be seen as a $3\sigma_g \rightarrow 1\sigma_u$ transition accompanied by a $3\sigma_g \rightarrow 1\pi_g$ "shake-up." This shake process is, however, not pronounced in photoemission [34] and x-ray absorption [37] on N_2.

In photoemission the $3\sigma_g^{-2}1\pi_g$ character has been assigned to a state found around 9 eV above the $3\sigma_g^{-1}$ state [35,36], and the $2\sigma_u^{-1}1\pi_u^{-1}1\pi_g^2$ states somewhat higher.

Although these final states are symmetry allowed and can be expected to be populated in the energy range where the spectral features are observed, they are not predicted to be the main configuration of the contributing states in the early calculation [16]. The definite assignment has to await further theoretical development and quantitative predictions.

The large width of the features can be due to both the short lifetime of the final states as their energy is in the valence ionization continua, and to their dissociative nature. The excitation-energy dependence can be simply modeled if the potential of the final state is strongly repulsive. With a linear repulsive potential in the Franck-Condon region the absolute square of the nuclear wave function in the intermediate state is directly imaged in the RIXS spectrum [38]. This is in line with the observations. Excitation to $v' = 0$ in the intermediate state results in broad Gaussian feature corresponding to the vibrational ground state. As higher vibrational excitations are reached the spectra become more complex, and they are eventually dominated by two features corresponding to the classical turning points. In the RIXS map such states thus get the shape of a V, with the tip corresponding to the equilibrium distance in the core excited state. Predictions using the simple model where the potential of the final state is assumed to be linear in the Franck-Condon region are shown in Fig. 4(c). The agreement with the observations is striking, giving credibility to the simple model. From the agreement we can also conclude that the lifetime width of the final state does not contribute much to the width of spectral features.

We also note an asymmetry in the V shaped structure which is not predicted by the simple theory [Fig. 4(c)]. Including LVI also in this model, as described in Ref. [38], reproduces an asymmetry and improves the agreement with the observations [Fig. 4(b)]. To account for the data we have used the final state potential $U_f(r) = U_0 + Sr$, where the slope $S = -24 \pm 2$ eV/Å, $U_0 = 48 \pm 3$ eV, r is the internuclear distance, and the errors are estimated by varying the parameters to the limits where the agreement with the experimental data significantly degrades.

The LVI influence implies that the imaging is sensitive to the scattering dynamics, especially the vibronic wave-function evolution in the intermediate state. In the theoretical difference spectra [Fig. 4(d)], we see that the interference effects introduce asymmetry by shifting intensity of the peak corresponding to the vibronic ground state towards higher energy losses for excitation just below the corresponding resonance, and towards lower energy losses for excitation just above. We also note that LVI effects emphasize the high-energy-loss part of the V shaped structure for excitation energies reaching highly excited vibronic states. This region is close to the equilibrium distance of the electronic ground state, which is not far from the classical inner turning point of the vibration in the intermediate state. In a time-dependent picture the LVI emphasis of this region can be related to the limited time given for the nuclear wave-function evolution in the intermediate state.

The weaker spectral feature at 13–14 eV energy loss [Fig. 4(a)] also seems to have a V shape, albeit with much smaller opening angle. Although the limited statistics makes conclusions more uncertain, this opening angle correspond to a slope of around 5 eV/Å, which we tentatively identify as the slope of the repulsive final state potential in the Franck-Condon region.

IV. CONCLUSION

We have presented RIXS spectra excited at the N_2 π^* resonance. Transitions to the electronic ground state and the state associated with the Lyman-Birge-Hopfield band are observed with vibrational resolution. Vibrational excitations are discussed using the Kramers-Heisenberg formalism, and LVI effects are highlighted. Although the two-step approximation is instrumental to grasp the crude phenomenology, LVI is

essential for the detailed comparison. In addition, we find two strongly dissociative multiply excited final states in the valence continua, populated via the $1\sigma_u^{-1}1\pi_g$ intermediate state due to RER in the second step. The notion that the intermediate state wave functions are imaged on a linear repulsive potential is used to determine its slope.

[1] L. Werme, B. Grennberg, J. Nordgren, C. Nordling, and K. Siegbahn, Observation of Vibrational Fine Structure in X-Ray Emission Lines, Phys. Rev. Lett. **30**, 523 (1973).

[2] M. Bässler, A. Ausmees, M. Jurvansuu, R. Feifel, J.-O. Forsell, P. de Tarso Fonseca, A. Kivimäki, S. Sundin, S. Sorensen, R. Nyholm *et al.*, Beam line I411 at MAX II—performance and first results, Nucl. Instrum. Methods Phys. Res. Sect. A **469**, 382 (2001).

[3] V. N. Strocov, T. Schmitt, U. Flechsig, T. Schmidt, A. Imhof, Q. Chen, J. Raabe, R. Betemps, D. Zimoch, J. Krempasky, X. Wang, M. Grioni, A. Piazzalunga, and L. Patthey, High-resolution soft X-ray beamline ADRESS at the Swiss Light Source for resonant inelastic X-ray scattering and angle-resolved photoelectron spectroscopies, J. Synchrotron Radiat. **17**, 631 (2010).

[4] S. Yamamoto, Y. Senba, T. Tanaka, H. Ohashi, T. Hirono, H. Kimura, M. Fujisawa, J. Miyawaki, A. Harasawa, T. Seike, S. Takahashi, N. Nariyama, T. Matsushita, M. Takeuchi, T. Ohata, Y. Furukawa, K. Takeshita, S. Goto, Y. Harada, S. Shin, H. Kitamura, A. Kakizaki, M. Oshima, and I. Matsuda, New soft X-ray beamline BL07LSU at SPring-8, J. Synchrotron Radiat. **21**, 352 (2014).

[5] S. Carniato, P. Selles, L. Andric, J. Palaudoux, F. Penent, M. Žitnik, K. Bučar, M. Nakano, Y. Hikosaka, K. Ito, and P. Lablanquie, Single photon simultaneous K-shell ionization and K-shell excitation. II. Specificities of hollow nitrogen molecular ions, J. Chem. Phys. **142**, 014308 (2015).

[6] L. Fang, T. Osipov, B. Murphy, F. Tarantelli, E. Kukk, J. P. Cryan, M. Glownia, P. H. Bucksbaum, R. N. Coffee, M. Chen, C. Buth, and N. Berrah, Multiphoton Ionization as a Clock to Reveal Molecular Dynamics with Intense Short X-Ray Free Electron Laser Pulses, Phys. Rev. Lett. **109**, 263001 (2012).

[7] R. Lindblad, L. Kjellsson, R. C. Couto, M. Timm, C. Bülow, V. Zamudio-Bayer, M. Lundberg, B. von Issendorff, J. T. Lau, S. L. Sorensen, V. Carravetta, H. Ågren, and J.-E. Rubensson, X-Ray Absorption Spectrum of the N_2^+ Molecular Ion, Phys. Rev. Lett. **124**, 203001 (2020).

[8] J.-E. Rubensson, M. Neeb, M. Biermann, Z. Xu, and W. Eberhardt, Electronic decay of vibrationally selected core excited states in molecular N_2, J. Chem. Phys. **99**, 1633 (1993).

[9] C. Miron, C. Nicolas, O. Travnikova, P. Morin, Y. Sun, F. Gel'mukhanov, N. Kosugi, and V. Kimberg, Imaging molecular potentials using ultrahigh-resolution resonant photoemission, Nat. Phys. **8**, 135 (2012).

[10] V. Kimberg, A. Lindblad, J. Söderström, O. Travnikova, C. Nicolas, Y. P. Sun, F. Gel'mukhanov, N. Kosugi, and C. Miron, Single-Molecule X-Ray Interferometry: Controlling Coupled Electron-Nuclear Quantum Dynamics and Imaging Molecu-

lar Potentials by Ultrahigh-Resolution Resonant Photoemission and *Ab Initio* Calculations, Phys. Rev. X **3**, 011017 (2013).

[11] P. Glans, P. Skytt, K. Gunnelin, J.-H. Guo, and J. Nordgren, Selectively excited X-ray emission spectra of N_2, J. Electron Spectrosc. Relat. Phenom. **82**, 193 (1996).

[12] J.-E. Rubensson, J. Söderström, C. Binggeli, J. Gråsjö, J. Andersson, C. Såthe, F. Hennies, V. Bisogni, Y. Huang, P. Olalde, T. Schmitt, V. N. Strocov, A. Föhlisch, B. Kennedy, and A. Pietzsch, Rydberg-Resolved Resonant Inelastic Soft X-Ray Scattering: Dynamics at Core Ionization Thresholds, Phys. Rev. Lett. **114**, 133001 (2015).

[13] M. N. Piancastelli, Auger resonant Raman studies of atoms and molecules, J. Electron Spectrosc. Relat. Phenom. **107**, 1 (2000).

[14] F. Hennies, A. Pietzsch, M. Berglund, A. Föhlisch, T. Schmitt, V. Strocov, H. O. Karlsson, J. Andersson, and J.-E. Rubensson, Resonant Inelastic Scattering Spectra of Free Molecules with Vibrational Resolution, Phys. Rev. Lett. **104**, 193002 (2010).

[15] J. Utriainen and T. Aberg, Two-electron jumps in the potassium Kβ X-ray spectrum, J. Phys. C **4**, 1105 (1971).

[16] H. Ågren, R. Arneberg, J. Müller, and R. Manne, X-ray emission of the nitrogen molecule following photon or electron impact. A theoretical study using configuration-interaction wavefunctions, Chem. Phys. **83**, 53 (1984).

[17] S. G. Chiuzbaian, C. F. Hague, A. Avila, R. Delaunay, N. Jaouen, M. Sacchi, F. Polack, M. Thomasset, B. Lagarde, A. Nicolaou, S. Brignolo, C. Baumier, J. Lüning, and J.-M. Mariot, Design and performance of AERHA, a high acceptance high resolution soft x-ray spectrometer, Rev. Sci. Instrum. **85**, 043108 (2014).

[18] M. Sacchi, N. Jaouen, H. Popescu, R. Gaudemer, J. M. Tonnerre, S. G. Chiuzbaian, C. F. Hague, A. Delmotte, J. M. Dubuisson, G. Cauchon, B. Lagarde, and F. Polack, The SEXTANTS beamline at SOLEIL: A new facility for elastic, inelastic and coherent scattering of soft X-rays, J. Phys. Conf. Ser. **425**, 072018 (2013).

[19] R. Feifel, M. Andersson, G. Öhrwall, S. L. Sorensen, M. N. Piancastelli, M. Tchaplyguine, O. Björneholm, L. Karlsson, and S. Svensson, A quantitative analysis of the N 1s$\rightarrow \pi*$ photoabsorption profile in N_2: new spectroscopical constants for the core-excited state, Chem. Phys. Lett. **383**, 222 (2004).

[20] K. Huber and G. Herzberg, *Molecular Structure and Molecular Spectra, Vol. 4. Constants of Diatomic Molecules* (Van Nostrand Reinhold, New York, 1979).

[21] F. Gel'mukhanov and H. Ågren, Resonant X-ray Raman scattering, Phys. Rep. **312**, 87 (1999).

[22] M. Neeb, J.-E. Rubensson, M. Biermann, W. Eberhardt, K. J. Randall, J. Feldhaus, A. L. D. Kilcoyne, A. M. Bradshaw, Z. Xu, P. D. Johnson, and Y. Ma, Effects of time evolution

of coherently excited vibrations in molecular core-hole decay spectra of O_2, Chem. Phys. Lett. **212**, 205 (1993).

[23] J. P. Dahl and M. Springborg, The Morse oscillator in position space, momentum space, and phase space, J. Chem. Phys. **88**, 4535 (1988).

[24] M. Neeb, J.-E. Rubensson, M. Biermann, and W. Eberhardt, Coherent excitation of vibrational wave functions observed in core hole decay spectra of O_2, N_2 and CO, J. Electron Spectrosc. Relat. Phenom. **67**, 261 (1994).

[25] K. Prince, M. Vondráček, J. Karvonen, M. Coreno, R. Camilloni, L. Avaldi, and M. De Simone, A critical comparison of selected 1s and 2p core hole widths, J. Electron Spectrosc. Relat. Phenom. **101**, 141 (1999).

[26] D. J. McEwen and R. W. Nicholls, Intensity distribution of the Lyman-Birge-Hopfield band system of N_2, Nature (London) **209**, 902 (1966).

[27] A. N. Nigam and S. N. Soni, Origin of low-energy satellites in K X-ray spectra. II. β-region, J. Phys. C **14**, 3289 (1981).

[28] J. Bonnet, A. Fleury, M. Bonnefoy, and L. Avan, Radiative auger emission in Ne K X-ray spectra, Phys. Lett. A **96**, 13 (1983).

[29] A. Kivimäki, M. Alagia, and R. Richter, X-ray emission–photoion coincidence spectroscopy of the CO2 molecule at the O 1s edge, Chem. Phys. Lett. **531**, 252 (2012).

[30] R. Couto, M. Guarise, A. Nicolaou, N. Jaouen, G. Chiuzbǎian, J. Lüning, V. Ekholm, J.-E. Rubensson, C. Såthe, F. Hennies, V. Kimberg, F. Guimarães, H. Agren, F. Gel'mukhanov, L. Journel, and M. Simon, English Anomalously strong two-electron one-photon X-ray decay transitions in CO caused by avoided crossing, Sci. Rep. **6**, 20947 (2016).

[31] G. Wendin, Collective effects, relaxation, and localization of hole levels in atoms, molecules, solids, and adsorbates, Int. J. Quantum Chem. **16**, 659 (1979).

[32] J.-I. Lo, M.-H. Tsai, H.-S. Fung, Y.-J. Chen, C.-C. Chu, T.-S. Yih, Y.-Y. Lee, C. Y. R. Wu, and D. L. Judge, Observation of new Rydberg series in the many-electron transition region of N_2, J. Chem. Phys. **137**, 054315 (2012).

[33] P. Gürtler, V. Saile, and E. Koch, High resolution absorption spectrum of nitrogen in the vacuum ultraviolet, Chem. Phys. Lett. **48**, 245 (1977).

[34] N. Kosugi, H. Kuroda, and S. Iwata, Breakdown of Koopmans' theorem and strong shake-up bands in the valence shell region of N_2 photoelectron spectra, Chem. Phys. **39**, 337 (1979).

[35] P. Baltzer, M. Larsson, L. Karlsson, B. Wannberg, and M. Carlsson Göthe, Inner-valence states of N_2^+ studied by uv photoelectron spectroscopy and configuration-interaction calculations, Phys. Rev. A **46**, 5545 (1992).

[36] A. J. Yencha, K. Ellis, and G. C. King, High-resolution threshold photoelectron and photoion spectroscopy of molecular nitrogen in the 15.0–52.7 eV photon energy range, J. Electron Spectrosc. Relat. Phenom. **195**, 160 (2014).

[37] E. Shigemasa, T. Gejo, M. Nagasono, T. Hatsui, and N. Kosugi, Double and triple excitations near the K-shell ionization threshold of N_2 revealed by symmetry-resolved spectroscopy, Phys. Rev. A **66**, 022508 (2002).

[38] F. Gelmukhanov and H. Ågren, X-ray resonant scattering involving dissociative states, Phys. Rev. A **54**, 379 (1996).

Correction: The surname of the eighth author contained a spelling error and has been fixed.